Comparison of Electromagnetic Performance of Superconducting Permanent Magnet Wind Power Generators with Different Topologies

Xiaoyan Huang, *Member, IEEE,* Chenxi Zhou, Kaihe Zhang, LijianWu, *Senior Member, IEEE,* Jian Zhang, *Member, IEEE,* and Wenping Cao, *Senior Member, IEEE*

***Abstract*—This paper mainly focuses on the comparison of electromagnetic performance of the superconducting permanent magnet (SCPM) generators with two different topologies. The torque capabilities of the two generators are first investigated. The peak torque is largely restricted by the material characteristics of the SC and the permanent magnet (PM). It turns out that the SCPM generators with iron-cored rotor and iron-cored stator topology (IRIST) is superior to the one with iron-cored rotor and air-cored stator topology (IRAST) in terms of torque capability. Furthermore, the flux density, line electromotive force (EMF), torque and its torque ripple, and the efficiency of the designed generators are evaluated by using numerical model. The simulation results confirm that IRIST has higher output torque and efficiency with the penalty of higher harmonics and torque ripples.**

***Index Terms*—Finite element method (FEM); superconducting permanent magnet wind power generator; topology; comparison**

I. INTRODUCTION

WIND energy, as a kind of clean energy, is developing rapidly these years. For wind turbine, large power wind turbine and direct drive wind turbine is also a good candidate [1]. That is to say, low-speed and high-torque generators are required, which indicate the main dimension would be large. It brings the challenges of the design in terms of high cost, difficulty in installation and maintenance.

The superconducting (SC) material can carry current density that is two orders of magnitude larger than that of copper [1], which can therefore lower the weight and size of the machine [2]. There are many researches on high temperature superconducting (HTS) generators. Shafaie and Kalantar have designed a 10-MW class HTS synchronous generator with rotor HTS field windings [3]-[4]. Kalsi researched fully superconducting wind turbine generator in [5]. Yi Cheng, *et al.* found that double-stator direct driving HTS wind generator has great advantages in volume and mass reduction [6]. A novel flux switching synchronous generator with HTS field windings is proposed in [7] and a large-scale wind turbine HTS synchronous generator is optimized and analyzed in [8].

The permanent magnet generator received intensive attention due to its high power density and high efficiency. However, few researches focused on PM generators with SC armature windings are reported in the previous literature. L. Li, *et al.* have designed the HTS PM motor with SC armature windings and found that the motor is competitive for its simple cooling sealing structure (no rotating cryogenic system) and high power density [9]-[10]. Furthermore, the advantages of HTS PM generators were proved through a prototype with copper winding instead of the HTS windings [11]. Kaihe Zhang has also analyzed HTS PM motor and compared it with the tradition copper PM motor [12]. It turns out that the HTS PM motor has higher power density and efficiency than the traditional copper PM motor.

This paper mainly focused on two topologies of superconducting permanent magnet (SCPM) generators, iron-cored rotor and stator topology (IRIST), iron-cored rotor and air-cored stator topology (IRAST). It is worth mentioning that there is still a magnetic yoke in stator for IRAST. The SCPM generator structures are presented in Section II in detail. Then, the optimization procedure for the two generators is carried out and the torque capabilities for the two generators are calculated and compared in Section III. Different aspects, including the flux density, electromotive force (EMF), torque performance and efficiency of the machines are investigated and compared in Section IV.

II. SCPM GENERATOR STRUCTURE

The structures of the two different SCPM generators are demonstrated in Fig. 1. The stator of the IRIST consists of an iron yoke and teeth, and SC armature windings while the stator teeth of the IRAST are made of non-magnetic material for the structural supporting and cooling of the SC armature windings. The cooling system composed of cryogenic system and cooling medium, surrounding the SC windings, is located in the stator slots. The rotors of the IRIST and IRAST are identical, including permanent magnets (PMs) and rotor iron core.

This work was supported by the National Natural Science Foundation of China under Grant 51477149 and 51690182.

Xiaoyan Huang, Chenxi Zhou, Kaihe Zhang, Lijian Wu and Jian Zhang are with the College of Electrical Engineering, Zhejiang University, China 310027 (e-mail: xiaoyanhuang@zju.edu.cn, 21610044@zju.edu.cn, 3100100854@zju.edu.cn, ljw@zju.edu.cn, jian_zhang_zju@zju.edu.cn,).

Wenping Cao is with Aston University, Birmingham United Kingdom, B4 7ET (e-mail: w.p.cao@aston.ac.uk).

This article has been accepted for publication in a future issue of this journal, but has not been fully edited. Content may change prior to final publication. Citation information: DOI 10.1109/TASC.2019.2895214, IEEE Transactions on Applied Superconductivity

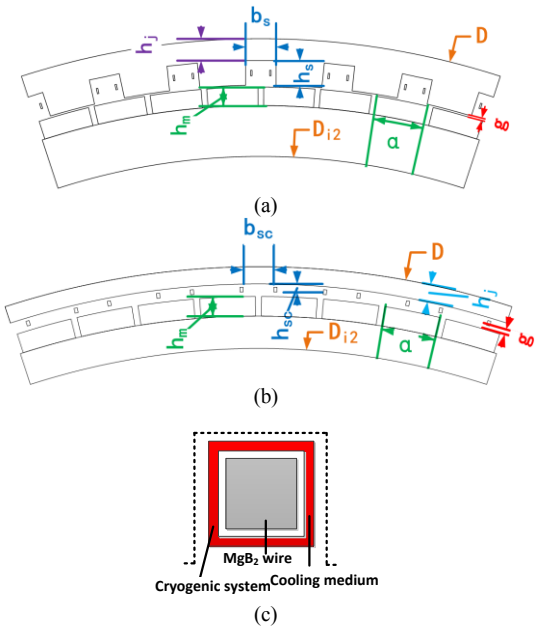

Fig. 1. Structures of SCPM generators. (a) IRIST. (b) IRAST. (c). Cross section of the cooling system located in stator slots. (D is the stator outer diameter, h_j is the stator yoke height, g is the active air gap length, h_m and α are the thickness and the angle of the PM, D_{i2} is the rotor inner diameter. For IRIST, b_s and h_s are the stator slot width and height. For IRAST, h_{sc} and b_{sc} are distance between the SC coil and the stator yoke and the distance between the adjacent SC coils in the virtual slot.)

III. Comparison Of Torque Capability

A. *Optimization procedure for SCPM generators*

To compare the two topologies of the SCPM generators, appropriate optimization for the generators is firstly carried out. The stator outer diameter, active length of the generators and pole number are identical for the two generators, set as 5m, 2 m and 80, respectively. Besides, the appropriate thickness of the PM, h_m and the angle of the PM, α are chosen and set as the same. The optimization process is carried out using Maxwell and the control strategy for the generators is set to id=0 [12].

The flowchart of the optimization procedure is demonstrated in Fig. 2. Different SC coil areas per slot (S_{sc}) are the primary and key parameters for the optimization procedure. The cross section area for each turn is the same, increasing SC coil areas per slot (S_{sc}) indicate higher number of turns.

With a specific S_{sc}, the optimization process mainly consists of two steps, the optimization for motor parameters (step I), and determination of the appropriate current density J_{sc} (step II).

For step I, optimization for motor parameters (h_j, h_s, b_s, h_{sc}, b_{sc}, g) as shown in Fig.1 is carried out to achieve the maximum torque with the same current supply.

For step II, in consideration of the material characteristics of the SC coils and the PMs, the process of determining appropriate J_{sc} is further separated into two parts, including calculation of critical quench current density and calculation of critical demagnetization current density. For calculation of critical quench current density, it is necessary to figure out the critical J_c-$B_\perp$ characteristic of the HTS. To guarantee the safe utilization of the SC material, a 25% safety margin is chosen as shown in Fig. 3. The MgB_2, developed by Hyper Tech, is adopted and the temperature is 30 K. The critical quench current density is calculated through the iteration shown in the flowchart. After that, the determined critical quench current density is further verified by the demagnetization performance. The minimum magnetic density B_{mag} is derived. The critical demagnetization current density goes down 10 A/mm^2 every time until the minimum B_{mag} is above 0.25 T. The appropriate current density J_{sc} is determined with the restriction of the material characteristics of both the HTS and PM.

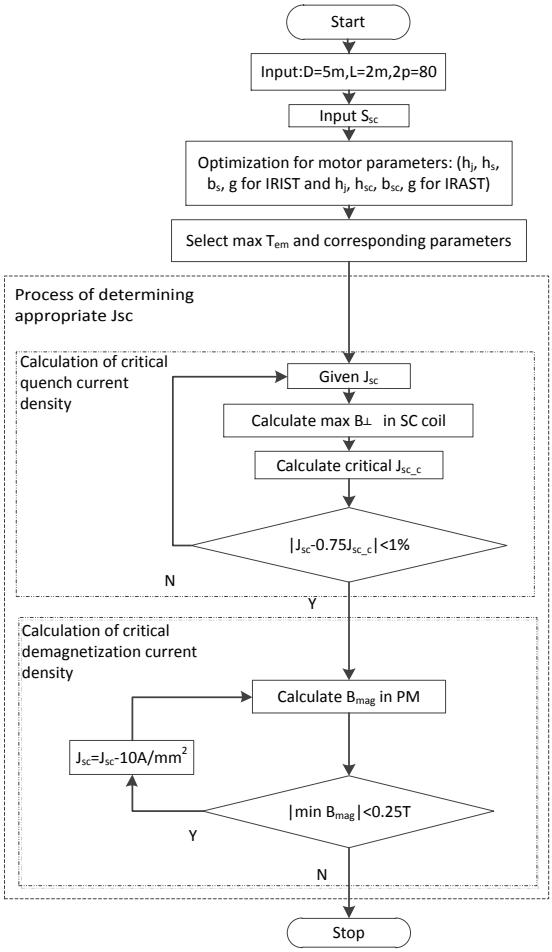

Fig. 2. The flowchart of the optimization procedure.

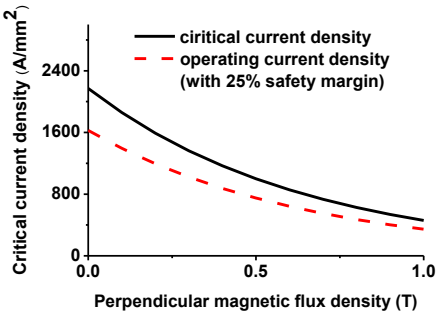

Fig. 3. The critical J_c-$B_\perp$ characteristic and its operating current density (with 25% safty margine) of the HTS (MgB_2) at 30 K.

This article has been accepted for publication in a future issue of this journal, but has not been fully edited. Content may change prior to final publication. Citation information: DOI 10.1109/TASC.2019.2895214, IEEE Transactions on Applied Superconductivity

B. *Torque capability of the SCPM generators*

The variations of the current density and the torque with the area of SC coil area per slot S_{sc} are shown in Fig. 4 and Fig. 5, respectively.

As shown in Fig. 4 and Fig. 5, both SCPM generators start to quench before demagnetize when the SC coil area per slot is below 520.8 mm^2 (region 1). When the SC coil per slot is above 520.8 mm^2 (region 2), the generators start to demagnetize firstly.

In region 1, the perpendicular flux density in the SC coil of the IRAST is bigger than that of the IRIST with the same armature current. Therefore, the maximum allowed current density before quench of the IRIST is bigger than that of the IRAST, as displayed in Fig. 4. Furthermore, the air gap flux density in IRIST is much higher than that of IRAST, as can be concluded from Fig. 7. Consequently, the torque of the IRIST generator is much higher than that of IRAST, as shown in Fig. 5.

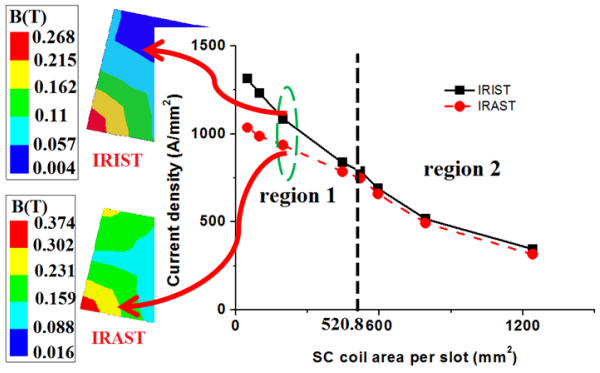

Fig. 4. The variations of the current density with SC coil areas per slot .

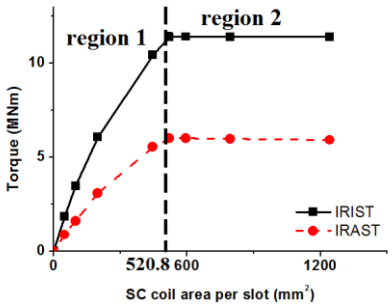

Fig. 5. The variations of the torque with SC coil areas per slot .

In region 2, the current density of the IRIST and IRAST is nearly the same. This means that the demagnetization of the PM has little relation with the slot of the stator part. It is mainly relevant to the design of the PM dimensions and the current applied to the SC coil, which are the source of the magneto motive force (MMF). To avoid the demagnetization of the PM, the MMF produced by the SC coil is restricted. With the rising of the SC coil area per slot, the maximum allowed current and the current density before demagnetization declined greatly. However, the torque of the generators remains a horizontal line in the demagnetization region due to the identical restricted MMF produced by the SC coil. The peak torque of the IRIST equals 11.5 MNm, much higher than that of the IRAST, around 6 MNm.

In conclusion, the IRIST is better than the IRAST for its better torque capability with the same constrained motor dimensions D and L.

IV. Comparison Of other performances

A. *Specification of the SCPM Generators*

To further compare the two topologies of the SCPM generators, the specific generators are designed. From Section II, the peak torque can be achieved when the SC coil area per slot is larger than 520.8 mm^2 for both SCPM generators. However, the rated voltage of the generators changes with the different SC coil area per slot. The rated voltage increases with the rising of the SC coil area per slot, as shown in Fig. 6. Thus, to meet the required rated voltage, the SC coil areas per slot for IRIST and IRAST are determined as 694.4 mm^2 and 1612 mm^2.

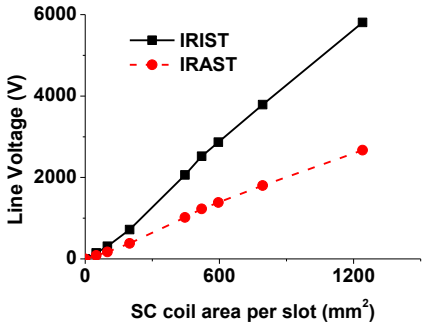

Fig. 6. The variations of the line voltage with SC coil areas per slot .

The specifications of the initial machines and optimized machines are shown in Table I.

TABLE I
SPECIFICATIONS OF SCPM GENERATORS

Parameter	Initial IRIST	Optimized IRIST	Initial IRAST	Optimized IRAST
Rated torque (MNm)	10.95	11.5	5.24	6
Rated output power (MW)	11.5	12	5.5	6.16
Rated voltage (Vrms)	3300	3300	3300	3300
Speed (rpm)	10	10	10	10
Frequency (Hz)	6.67	6.67	6.67	6.67
Operating temperature (K)	30	30	30	30
Outer diameter D (mm)	5000	5000	5000	5000
Active length L (mm)	2000	2000	2000	2000
Number of poles	80	80	80	80
h_m (mm)	60	60	60	60
α (°)	4.05	4.05	4.05	4.05
PM material	N35H	N35H	N35H	N35H
g (mm)	6	6	15	15
h_j (mm)	120	90	80	40
h_s (mm)	100	80	/	/
b_s (mm)	87	97	/	/
h_{sc} (mm)	/	/	55	42
b_{sc} (mm)	/	/	5	10
Area of SC coil per slot (mm^2)	694.4	694.4	1612	1612
Current density (A/mm^2)	591	591	263	263
Power factor	0.43	0.5	0.57	0.605

This article has been accepted for publication in a future issue of this journal, but has not been fully edited. Content may change prior to final publication. Citation information: DOI 10.1109/TASC.2019.2895214, IEEE Transactions on Applied Superconductivity

B. No load Flux Density and Line EMF

Fig. 7 shows the waveforms of the flux density in the middle of the air-gap and its harmonic component under no-load circumstance. Fig. 8 shows the waveforms of the rated-load line electromotive force (EMF) and its harmonic component. The results of the different generators are put together for clearer comparison.

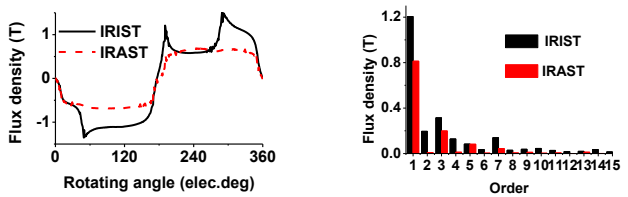

Fig. 7. No-load flux density in the air-gap. (a)Waveforms. (b) Fourier decomposition.

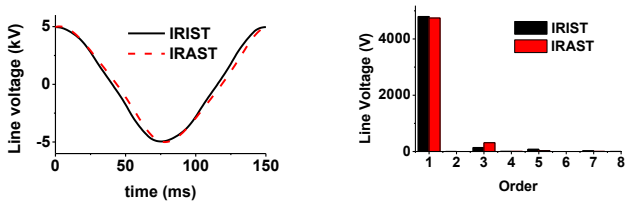

Fig. 8. Rated-load line EMF. (a)Waveforms. (b) Fourier decomposition.

From Fig. 7, it is easy to find out that the flux density of the IRAST under no-load circumstances has smoother waveform without the influence of the stator iron teeth. And the Fourier waveform further demonstrates that the flux density of the IRAST has lower harmonic and less harmonic components. The average air-gap flux density of the IRIST is much higher than that of the IRAST. For the line-EMF under rated-load, the waveforms are similar and smooth for both generators.

C. On-Load Torque and Torque Ripple

The rated torque waveforms and its spectra are shown in Fig. 9. The average torque of the IRIST is around 2 times as the torque of IRAST. However, the torque ripple of IRIST is 5.1%, twice as large as the IRAST, around 2.6%. The result confirms that the removal of the stator slots reduced the torque ripple greatly.

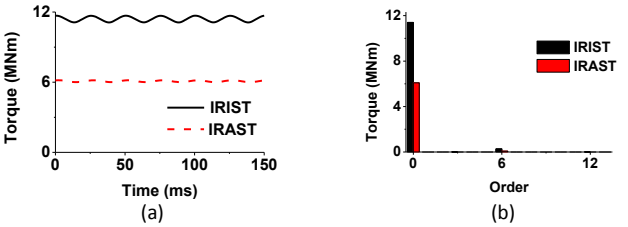

Fig. 9. Rated torque. (a)Waveforms. (b) Fourier decomposition.

D. Loss Analysis and efficiency

To calculate the efficiency of the generators, loss analysis is important, as can be inferred from (1). For SCPM generators, the loss includes three parts, iron loss, AC loss and cryogenic power.

$$\eta = \frac{T_{em}\Omega - P_{iron} - P_{AC} - P_{cry}}{T_{em}\Omega} \tag{1}$$

Where, T_{em} is the electromagnetic torque, Ω is the mechanical speed, P_{iron} is the iron loss, P_{AC} is the AC loss, P_{cry} is the cryogenic power.

For IRIST, the heavier iron mass and the higher flux density due to the extra teeth structure lead to the larger iron loss, which equals 9.3009 kW. For IRAST, the iron loss values 2.1531 kW, less than one fourth of the iron loss of the IRIST.

The AC loss in SC winding consists of magnetic hysteresis loss P_h and eddy-current loss P_e, as can be expressed from (2)-(5), [13]-[15].

$$P_{AC} = P_h + P_e \tag{2}$$

$$Q_h = \begin{cases} \dfrac{2B_p^{\,2}}{3\mu_0}(i^3 + 3\beta^2 i) & (\beta < i) \\ \dfrac{2B_p^{\,2}}{3\mu_0}(\beta^3 + 3\beta i^2) & (i < \beta < 1) \\ \dfrac{2B_p^{\,2}}{3\mu_0}(\beta(3+i^2) - 2(1-i^3) & \\ +6i^2\dfrac{(1-i)^2}{(\beta - i)} - 4i^2\dfrac{(1-i)^3}{(\beta - i)^2}) & (\beta > 1) \end{cases} \tag{3}$$

$$P_h = Q_h \times L_{sc} \times A_{sc} \times f \tag{4}$$

$$P_e = \frac{4\pi^2 f \tau B_a^{\,2}}{\mu_0(1 + 2\pi f \tau)^2} \times L_{sc} \times A_{sc} \times f \times \frac{1-r}{r} \tag{5}$$

Where, Q_h is the magnetic hysteresis loss coefficient, B_a is the amplitude of the magnetic field and B_p is the field of full penetration of a slab, $\beta = B_a/B_p$ is the normalized magnetic field, I_t and I_c are the amplitude transport current and the critical current, $i = I_t/I_c$ is the normalized transport current, f is the frequency, L_{sc} and A_{sc} are length and area of the SC windings, τ is the intrinsic time, r is the SC area ratio and μ_0 is the absolute permeability.

The AC loss of the IRAST and IRIST are around 3.18kW and 1.40kW respectively. The AC loss mainly relates to the flux density in the SC coil and the usage amount of the SC coil. For the two generators, the flux density induced in the SC coil is close. However, the usage amount of the SC coil for IRAST is nearly two times of the IRIST. The cryogenic power is proportional to the AC loss, as deduced from (6), which means the cryogenic power for IRIST is also smaller.

$$P_{cry} = 36 P_{AC} \tag{6}$$

The total loss of the two generators is 119.64 kW for IRAST and 61.35 kW for IRIST. Thus, the efficiency of the IRIST values 99.49% while the efficiency of the IRAST equals 98%.

V. Conclusions

In this paper, SCPM generators with two different topologies are designed, optimized and compared. With the same dimensions of the out stator diameter and the active length, the optimized IRIST has higher no-load flux density in air gap than the IRAST, owing to the smaller air gap length. This also contributes to the higher torque capability for IRIST under the same restriction of the material characteristics of the SC coil and PM. When both generators are operated under the critical demagnetization condition to achieve the peak torque, the flux density in the SC coil is close. However, with larger usage amount of the SC coil, AC loss and cryogenic power for IRAST is higher, leading to the lower efficiency.

In conclusion, IRIST SCPM generator has better output torque capability and higher efficiency than IRAST. However, the harmonics of the no-load air gap flux density of the IRAST is much less and its torque ripple is smaller owing to the removal of the stator teeth for IRAST.

References

[1] Y. Guan et al., "Comparison of Electromagnetic Performance of 10-MW Superconducting Generators With Different Topologies for Offshore Direct-Drive Wind Turbines," in IEEE Transactions on Applied Superconductivity, vol. 27, no. 7, pp. 1-11, Oct. 2017.

[2] Z. Deng et al., "Pulsed Field Magnetization Properties of Bulk RE-Ba-Cu-O as Pole-Field Magnets for HTS Rotating Machines," in IEEE Transactions on Applied Superconductivity, vol. 21, no. 3, pp. 1180-1184, June 2011.

[3] R. Shafaie and M. Kalantar, "Loss optimization of a 10 MW class HTS synchronous generator based wind turbines," 2014 14th International Conference on Environment and Electrical Engineering, Krakow, 2014, pp. 29-33.

[4] R. Shafaie and M. Kalantar, "Design of a 10-MW-Class Wind Turbine HTS Synchronous Generator With Optimized Field Winding," in IEEE Transactions on Applied Superconductivity, vol. 23, no. 4, pp. 5202307-5202307, Aug. 2013.

[5] S. S. Kalsi, "Superconducting Wind Turbine Generator Employing MgB2 Windings Both on Rotor and Stator," in IEEE Transactions on Applied Superconductivity, vol. 24, no. 1, pp. 47-53, Feb. 2014.

[6] Y. Cheng, D. Li, W. Kong, R. Qu and F. Lin, "Electromagnetic Design of a Large-Scale Double-Stator Direct Driving HTS Wind Generator," in IEEE Transactions on Applied Superconductivity, vol. 28, no. 4, pp. 1-5, June 2018, Art no. 5205105.

[7] Y. J. Hwang et al., "Electromagnetic Design of a 15 MW-Class HTS Flux Switching Synchronous Generator considering Mechanical Stress of the Rotor Core," in IEEE Transactions on Applied Superconductivity, vol. 24, no. 3, pp. 1-5, June 2014, Art no. 5202305.

[8] Y. Xu, N. Maki and M. Izumi, "Optimization Study of Machine Parameters for 10-MW Salient-Pole Wind Turbine HTS Generators," in IEEE Transactions on Applied Superconductivity, vol. 26, no. 3, pp. 1-5, April 2016, Art no. 5203405.

[9] L. Li, J. Cao, B. Kou, Z. Han, Q. Chen and A. Chen, "Design of the HTS Permanent Magnet Motor With Superconducting Armature Winding," in IEEE Transactions on Applied Superconductivity, vol. 22, no. 3, pp. 5200704-5200704, June 2012.

[10] A. Chen, X. Liu, F. Xu, J. Cao and L. Li, "Design of the Cryogenic System for a 400 kW Experimental HTS Synchronous Motor," in IEEE Transactions on Applied Superconductivity, vol. 20, no. 3, pp. 2062-2065, June 2010.

[11] L. Li, J. Cao, B. Kou, S. Yang, D. Pan and H. Zhu, "Design of Axial and Radial Flux HTS Permanent Magnet Synchronous Motor's Rotor," in IEEE Transactions on Applied Superconductivity, vol. 20, no. 3, pp. 1060-1062, June 2010.

[12] K. Zhang et al., "Design of a 10 MW dual-stator superconducting permanent magnet wind power generator," 2016 19th International Conference on Electrical Machines and Systems (ICEMS), Chiba, 2016, pp. 1-4.

[13] J. J. Rabbers, D. C. van der Laan, B. ten Haken and H. H. J. ten Kate, "Magnetisation and transport current loss of a BSCCO/Ag tape in an external AC magnetic field carrying an AC transport current," in IEEE Transactions on Applied Superconductivity, vol. 9, no. 2, pp. 1185-1188, June 1999.

[14] M.N.Wilson, Superconducting Magnets, CLARENDON PRESS OXFORD, Ch.8, 1983.

[15] N. Magnusson, A.B. Abrahamsen, D. Liu, M. Runde, H. Polinder, Hysteresis losses in MgB2 superconductors exposed to combinations of low AC and high DC magnetic fields and transport currents, Physica C: Superconductivity and its Applications, Volume 506, 2014, Pages 133-137, ISSN 0921-4534, https://doi.org/10.1016/j.physc.2014.06.012.